

www.acsnano.org

# Stability of Protein Structure during Nanocarrier Encapsulation: Insights on Solvent Effects from Simulations and Spectroscopic Analysis

Chester E. Markwalter, Betul Uralcan, István Pelczer, Shlomo Zarzhitsky, Michael H. Hecht, Robert K. Prud'homme,\* and Pablo G. Debenedetti\*



Cite This: https://dx.doi.org/10.1021/acsnano.0c06056



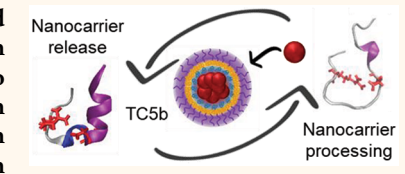
**ACCESS** 

III Metrics & More



Supporting Information

ABSTRACT: The dosing of peptide and protein therapeutics is complicated by rapid clearance from the blood pool and poor cellular membrane permeability. Encapsulation into nanocarriers such as liposomes or polymersomes has long been explored to overcome these limitations, but manufacturing challenges have limited clinical translation by these approaches. Recently, inverse Flash NanoPrecipitation (iFNP) has been developed to produce highly loaded polymeric nanocarriers with the peptide or protein contained within a hydrophilic core, stabilized by a hydrophobic polymer shell.



Encapsulation of proteins with higher-order structure requires understanding how processing may affect their conformational state. We demonstrate a combined experimental/simulation approach to characterize protein behavior during iFNP processing steps using the Trp-cage protein TC5b as a model. Explicit-solvent fully atomistic molecular dynamics simulations with enhanced sampling techniques are coupled with two-dimensional heteronuclear multiple-quantum coherence nuclear magnetic resonance spectroscopy (2D-HMQC NMR) and circular dichroism to determine the structure of TC5b during mixed-solvent exposure encountered in iFNP processing. The simulations involve atomistic models of mixed solvents and protein to capture the complexity of the hydrogen bonding and hydrophobic interactions between water, dimethylsulfoxide (DMSO), and the protein. The combined analyses reveal structural unfolding of the protein in 11 M DMSO but confirm complete refolding after release from the polymeric nanocarrier back into an aqueous phase. These results highlight the insights that simulations and NMR provide for the formulation of proteins in nanocarriers.

KEYWORDS: molecular dynamics, nanocarrier, protein delivery, simulations, spectroscopy

eptide and protein therapeutics, which are also termed biologics or biopharmaceuticals, constitute a significant, and growing, portion of the pharmaceutical market. The rate of new product approvals for biologics nearly doubled during the period since 2015 as compared to an essentially constant rate from 1995 through 2014. Whereas biologics are potent and specific drugs, their clinical translation faces challenges in administration that must be addressed to realize the field's potential. Biologics typically possess physical properties that limit transport across the epithelium and require injection to achieve clinically relevant bioavailability.<sup>2,3</sup> Protease activity and filtration clearance mechanisms result in half-lives in circulation as short as minutes; therefore, frequent dosing is required.4-6 Encapsulation can impart protection from protease activity prior to release and promote cell internalization.3 Consequently, a range of technologies have been employed to produce particulate formulations, including liposomes and the double emulsion approach to produce polymer nanocarriers (NCs).<sup>5,7</sup>

There are significant processing challenges with these techniques.<sup>8</sup> We have recently presented an encapsulation approach that enables encapsulation efficiencies and drug loadings in NCs higher than those of any previous method. The technique, inverse Flash NanoPrecipitation (iFNP), has been demonstrated for peptides, oligonucleotides, and proteins.<sup>9</sup> The iFNP process uses rapid mixing and precipitation in specific mixing geometries to assemble "inverse nanocarriers" containing a water-soluble therapeutic within a

Received: July 20, 2020 Accepted: November 9, 2020



ACS Nano www.acsnano.org Article

hydrophilic core that is stabilized by an amphiphilic block copolymer in a hydrophobic external solvent (Figure 1).

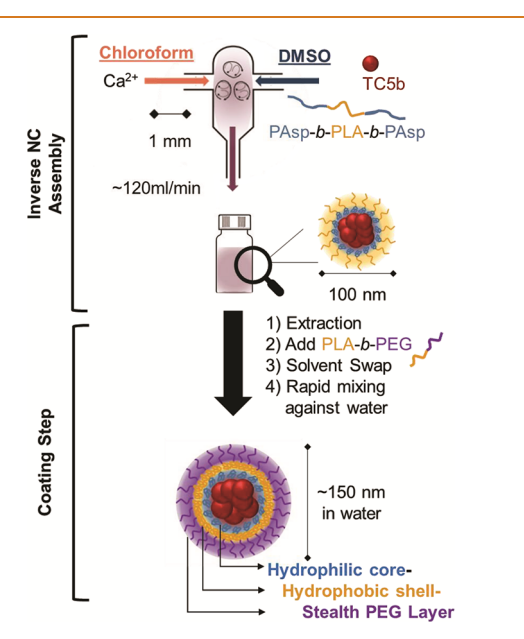


Figure 1. Processing schematic showing the assembled NC structure at each step, in exaggerated detail. A confined impinging jet (CIJ) mixer was used in the iFNP step to form inverse NCs. After crosslinking, residual dimethylsulfoxide was removed in an extraction and the water-immiscible chloroform was exchanged by solvent swap to tetrahydrofuran. This stream, with PLA-b-PEG added, was then rapidly mixed with water in the CIJ to collapse the PLA shell and coat the inverse NCs with the PLA-b-PEG block copolymer. The internal geometry of the CIJ mixer is depicted in the iFNP step with schematic turbulent mixing shown.

Nanocarrier assembly is initiated by solubility changes during mixing that drive the biologic and the polar polymer block out of solution. The hydrophobic block remains solvated in the external organic phase and provides steric stabilization. <sup>10–13</sup>

Here, we employed a stabilizer, comprising a hydrophobic poly(lactic acid) block and highly soluble poly(aspartic acid) blocks: PAsp<sub>Sk</sub>·b-PLA<sub>10k</sub>·b-PAsp<sub>Sk</sub>. The PAsp blocks comprise the core, along with the biologic. The PAsp is ionically crosslinked with a metal cation such as Ca<sup>2+</sup> to stabilize the inverse NCs during subsequent processing. The hydrophobic PLA block forms the stabilizing polymer brush. A second coating step installs PLA-b-PEG onto this surface, creating highly loaded NCs with sizes around 100 nm.<sup>9</sup>

However, there are still significant unknowns for protein therapeutics in the process because they require retention of their native structure upon release. It is well-known that exposure to organic solvents can be detrimental to protein structure and activity, with water-miscible organic solvents exhibiting particularly strong effects in some cases. Understanding protein structure in these mixed-solvent systems is crucial for developing effective protein NC processes for therapeutics. The iFNP process employs amphiphilic polymers to achieve the inverse NC architecture. The polymer must be solubilized with solvents such as dimethylsulfoxide (DMSO), resulting in exposure of the protein to potentially destabilizing conditions.

We studied the 20-residue Trp-cage miniprotein (TC5b) because it exhibits features found in larger globular proteins such as a stable tertiary structure with a hydrophobic core, a salt bridge, an  $\alpha$ -helix, and a  $3_{10}$ -helix. Furthermore, its rapid (microsecond scale) folding behavior has been extensively characterized by experiment and simulation. First, we demonstrate that TC5b can be encapsulated by iFNP to produce 50 wt % loaded inverse NCs and then coated with a PEG block copolymer for *in vivo* administration. We then employ atomistic simulations, nuclear magnetic resonance (NMR), and circular dichroism (CD) to generate insight into the physical state of the biologic during processing.

Atomistic simulations that correctly account for solvent—protein interactions are essential to understanding the population-specific denaturing and refolding process. Realistic force fields must be employed to accurately compare

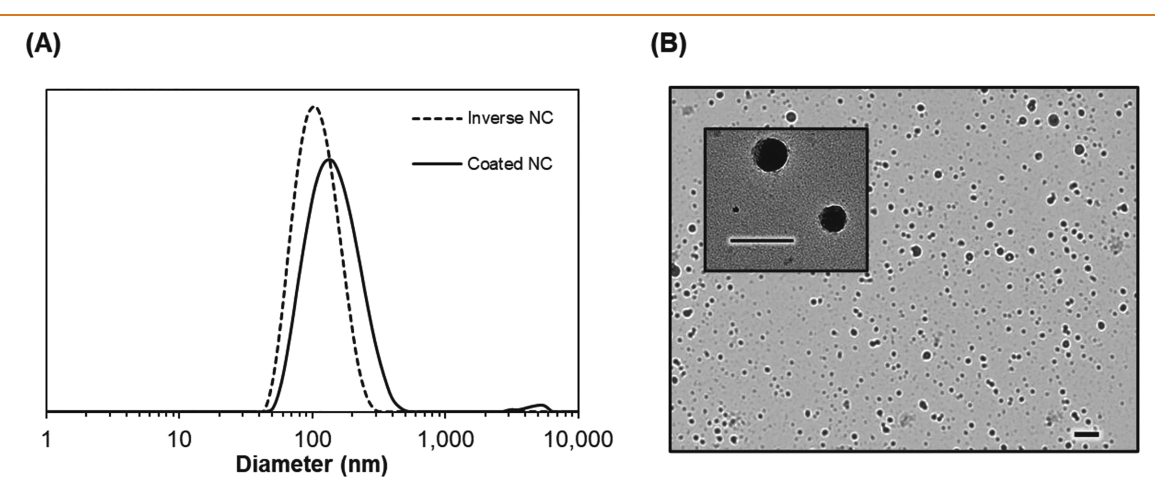


Figure 2. (A) Dynamic light scattering (DLS) traces showing the hydrodynamic diameter of TC5b polymeric NCs after iFNP (dashed line) and PLA-b-PEG coating (solid line). A small dust/aggregate population can be seen in the coating trace, which can be minimized by modified processing conditions. (B) Micrograph of coated NCs stained with ruthenium. Scale bars are 500 nm for the wide-angle image and 200 nm for the inset. The inset depicts the spherical particles and the presence of a small micelle population, reflecting excess PLA-b-PEG used in the formulation. The image is of coated NCs produced with purified PAsp<sub>5k</sub>-b-PLA<sub>10k</sub>-b-PAsp<sub>5k</sub>, with a DLS intensity-weighted size of 218 nm. The apparent smaller size by transmission electron microscopy reflects dehydration during grid preparation as well as the bias of intensity-weighted DLS size distributions towards larger particle populations relative to the number-weighted distributions observed by microscopy.

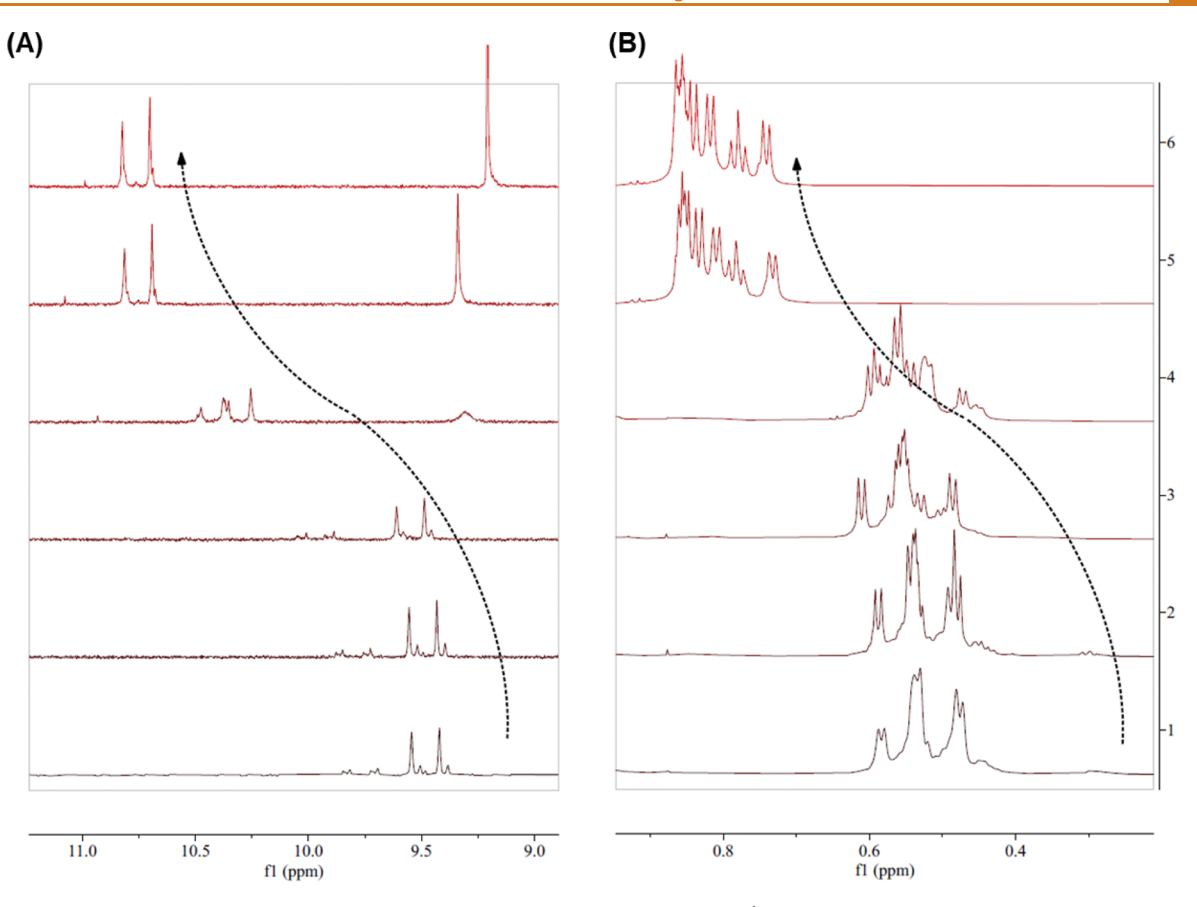


Figure 3. Stacked plot of DMSO/water mixtures with increasing DMSO concentration (named according to Table 1, from bottom to the top: 0, 1, 5, 11, 13.5 M, and pure DMSO). Only characteristic regions of the (A) Trp imino proton and (B) upfield methyl resonances are shown. The spectra were calibrated using peaks of small contaminants with stable chemical shifts regardless of the large span of solvent conditions. Both regions show characteristic change of downfield chemical shifts from largely folded conditions (bottom) to fully unfolded (top). The iFNP input composition is typically 13.5M DMSO (90–95 vol %).

simulations to experimental data. Therefore, as will be presented below, protein and water molecules were modeled using Amber03w and the TIP4P/2005 force fields that yield excellent agreement with experiment in terms of predicting the Trp-cage's folding kinetics and intermediate states. 20–23 1D and 2D band-Selective Optimized Flip-Angle Short-Transient heteronuclear multiple quantum coherence (SOFAST-HMQC) experiments elucidated the TC5b structure under steady-state conditions as a function of DMSO volume fraction. The simulations and NMR experiments were in quantitative agreement. Although this model protein is small, the approach presents a path forward to understand protein stability for larger proteins during iFNP processing by leveraging complementary advanced simulations coupled with experimental measurements of protein activity and structure.

# **RESULTS AND DISCUSSION**

# Whereas the synthetic version of TC5b is readily available, structural studies employing NMR require a uniformly isotopically labeled material, which is best achieved by the expression of the peptide *in vivo*. To produce a uniformly labeled <sup>15</sup>N version of TC5b (<sup>15</sup>N-TC5b), we utilized the *de*

Preparation of <sup>15</sup>N-TC5b by Recombinant Expression.

novo expression enhancer protein (DEEP). This fusion tag showed superior TC5b expression yields when compared to SUMO.<sup>24</sup> HPLC fractions of cleaved <sup>15</sup>N-TC5b after DEEP expression were lyophilized and then pooled in a second

lyophilization process from deionized water. Isolation of purified material was confirmed by HPLC, MS, and CD. The <sup>15</sup>N-labeled protein produced a single peak by HPLC, with retention time matching the unlabeled material generated by solid-state synthesis. The peak had a mass that corresponded to 96% labeling by MS (26 of 27 nitrogen atoms). The CD spectrum was an excellent match for the unlabeled TC5b (Figure S1). The <sup>15</sup>N-TC5b was used in subsequent experiments and will be referenced simply as "TC5b" below.

TC5b Formulates Readily into Water-Dispersible Polymeric NCs. Inverse NCs encapsulating TC5b at up to 50 wt % were prepared in a confined impinging jet (CIJ) mixer with high reproducibility and narrow particle size (Figure 2A). The inverse NC dispersions were visually clear and free of aggregates with intensity-weighted size of 105 ± 7 nm and polydispersity index (PDI) of 0.12  $\pm$  0.05. Residual DMSO was removed by extracting the chloroform dispersion with 150 mM NaCl in water. To further confirm that TC5b was encapsulated inside the inverse NCs, the TC5b concentration in the aqueous phase of the extraction was determined by the bicinchoninic acid assay using standard procedures. Unencapsulated TC5b removed in the extraction step was only 1.5  $\pm$ 0.4% of the input, indicating an initial encapsulation efficiency of over 98%. Controls without the block copolymer produced large, extractable aggregates.

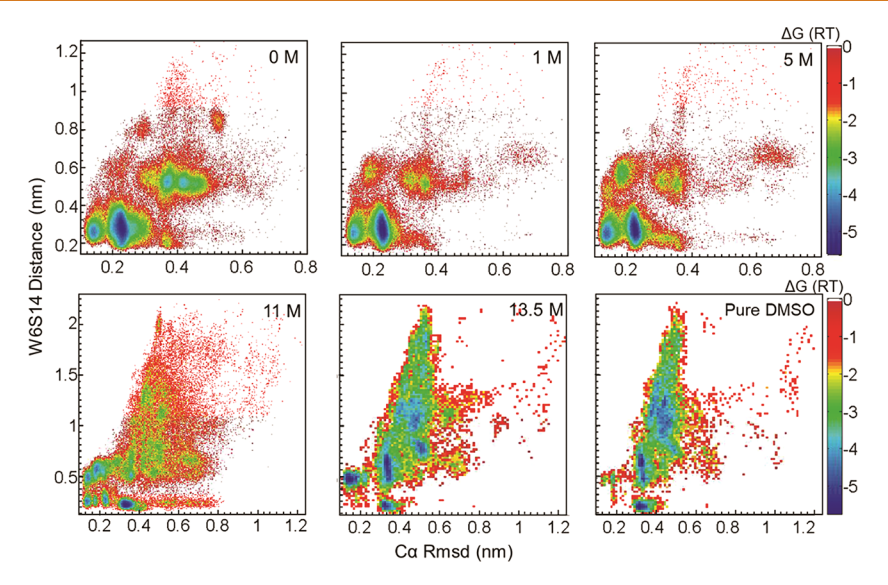


Figure 4. Free energy surfaces associated with the order parameters  $C\alpha$  rmsd and W6-S14 distance for DMSO/water mixtures with increasing DMSO concentration (0, 1, 5, 11, 13.5 M, and pure DMSO). The surfaces show a clear transition at 11 M.

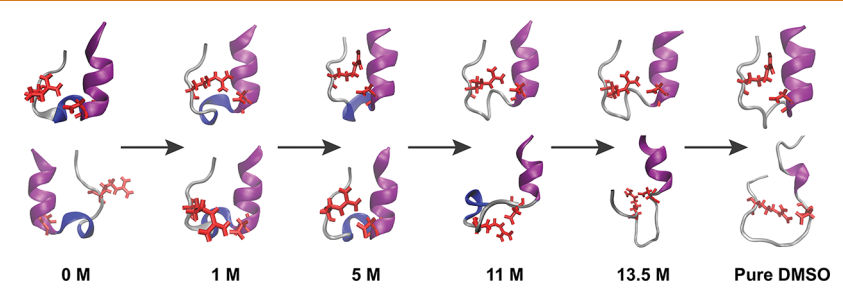


Figure 5. Representative protein configurations from the most populated two clusters in 0, 1, 5, 11, 13.5 M, and pure DMSO. Trp-cage's  $\alpha$ -helix,  $3_{10}$ -helix, and aromatic side chain on residue W6 are rendered in purple, blue, and red, respectively.

To produce PEG-coated, water-dispersible NCs, the solvent was exchanged with tetrahydrofuran (THF), and a PEG steric coating layer was applied by passing the NCs through a second FNP process to assemble a PLA-b-PEG polymer on the inverse NC surface. In this step, an aqueous antisolvent stream drives the PLA block assembly onto the NC surface. Hydrodynamic size increased after coating to 166 ± 11 nm, and the PDI increased to 0.22  $\pm$  0.05. This increased PDI may reflect a fraction of the PLA-b-PEG assembling into micelles rather than coating inverse NCs during the CIJ mixing process (see Figure 2B, inset).9 The zeta-potential of the coated NCs was significantly more neutral than controls without the PEG block copolymer (-7.2  $\pm$  2.7 and -42  $\pm$  0.9 mV, respectively). These results indicate the attachment of the PEG layer on the NC surface. The strong negative charge observed in the absence of the PEG block copolymer arises because the highly charged PAsp block is exposed on the NC surface if the second PLA-b-PEG layer is not applied. The target loading of the coated NC was 26 wt % by mass; with protein losses during the coating step, the final protein loading was 4 wt %. This is lower than has been observed for other proteins in iFNP, where loading has been demonstrated up to 27 wt %. However, as the purpose of this experiment was to assess protein stability upon mixed-solvent exposure, the process was not further optimized to improve protein loading efficiency.

Unfolding of TC5b in DMSO/Water Input to iFNP. The unfolding behavior of TC5b in the DMSO/water solutions,

required for inverse NC formation, was evaluated by MD simulations and NMR, generated with 1D <sup>1</sup>H and 2D SOFAST-HMQC experiments. Proton NMR spectra for the imino and methyl regions are shown in Figure 3. HMQC spectra in the amide region reveal similar behavior (Figure S2). There is a clear inflection point or transition regime observed at 11 M DMSO (condition 4, 78 vol % DMSO), where the folded species transition to largely unfolded ones, in full agreement with the MD simulations, and undergo increasing scales of mobility, leading to line broadening. The samples with no or low concentration of DMSO have at least five visible TC5b components, although one (with the smallest concentration) might be a different, but closely related, molecule which remains visible at 100 vol % DMSO, as well. The fact that these components have relatively sharp peaks in close proximity to each other suggests that the individual conformers have relatively long lifetimes and are kinetically

These results were in close agreement with the MD simulations of TC5b. Whereas NMR experiments capture the principal thermodynamic signatures of DMSO-induced perturbations in TC5b's structure, fully atomistic simulations give additional insight by providing a detailed microscopic description. To this end, changes in TC5b's overall structure were characterized by constructing the free energy surfaces associated with the order parameters  $C\alpha$  rmsd and W6S14 distance using the simulation data. Figure 4 shows these free energy surfaces at 300 K for 0, 1, 5, 11, 13.5 M, and pure

DMSO. At DMSO concentrations lower than 11 M, multiple basins corresponding to distinct TC5b configurations are observed, in agreement with NMR experiments. The free energy surface at 0 M depicts two basins that correspond to folded TC5b configurations ( $C\alpha$  rmsd < 0.3 nm, W6S14 distance < 0.42 nm) and multiple other shallower basins that correspond to partially unfolded configurations. The representative conformations of the two folded minima differ only by the presence of an N-terminal backbone hydrogen bond between asparagine (N1O) and glutamine (Q5H) residues. This is in line with previous NMR data that identify native TC5b configurations with a stable or a broken N-terminal backbone hydrogen bond (N1O–Q5H).

The simulations reveal that the folded basins remain stable up to 11 M DMSO (78 vol %). Above 11 M, the equilibrium of conformational states shifts toward unfolded states, whereas the basins with folded states become shallower. As depicted in Figure 5, the unfolded states are distinguished from the folded states by the destabilization of TC5b native secondary and tertiary structure elements, including the N-terminal  $\alpha$ -helix, which becomes partially unfolded in a large subset of the accessible configurations. These states become increasingly populated as the DMSO concentration is increased above 11 M until they dominate the free-energy landscape in pure DMSO. The significant shift in TC5b solvent-accessible surface area and radius of gyration at 11 M also indicate the clear transition at high DMSO concentrations (Figure 6).

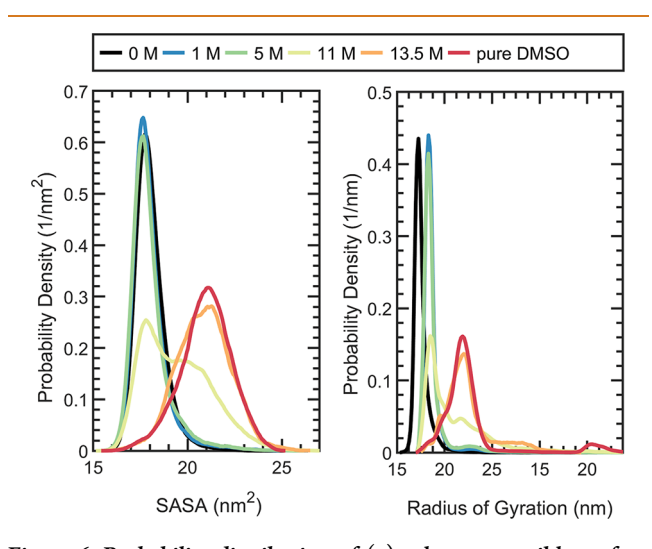


Figure 6. Probability distribution of (a) solvent-accessible surface area (nm²) and (b) radius of gyration [0 M (black), 1 M (blue), 5 M (green), 11 M (yellow), 13.5 M (orange), and pure DMSO (red)].

Our fully atomistic molecular simulations also indicate that DMSO-induced destabilization exhibits significant differences from complete unravelling that occurs in the case of heat denaturation. This becomes evident upon comparing the free-energy surface of TC5b at a heat-denatured state, which exhibits complete structural loss (Figure S3), and the free energy surfaces at high DMSO concentrations in which the  $\alpha$ -helix of TC5b remains partially stable while the salt bridge between aspartic acid (D9) and arginine (R16) becomes even more pronounced (Figure S4). The representative configurations in Figure 5 also illustrate the stable salt bridge at high DMSO concentrations. Our attempt to identify this stabilized

D9-R16 salt bridge by NMR was not successful given the complexity of the spectrum, which exhibited multiple exchanging components and the likely short kinetic lifetime of the salt bridge, and the naturally limited possibly observable NOE contacts. Identification of any direct contact by NOE would be very difficult due to a lack of sufficiently short proton—proton distances.

For iFNP, the input stream containing the biologic is DMSO at 90 vol % or greater to ensure that the PAsp-b-PLA is molecularly dissolved. Lower DMSO content can result in micellization of the polymer, adversely impacting the assembly of NCs in the mixing process. These results clearly indicate loss of the native TC5b state in the encapsulation process. Nevertheless, a formulation that permits refolding of the encapsulated protein either *in situ* or upon release can still be therapeutically efficacious. Therefore, we sought to determine whether the processed TC5b is released from coated NCs in a folded state.

TC5b Refolds after iFNP Processing. We found that low levels of free PAsp homopolymer in the PAsp-b-PLA block copolymer interfered with CD characterization of TC5b after processing. We therefore purified the block copolymer using an aqueous precipitation from DMSO. Formulations with the purified block copolymer processed similarly, though the coated NCs were slightly larger (218 nm). Ultrafiltration through a 50 kDa membrane was used to separate free TC5b that diffused from the inverse NC during coating. Figure 7A shows the HPLC chromatogram of TC5b before and after processing by iFNP, confirming the chemical identity of the TC5b and minimal purity change during processing. The structural features of the free TC5b were assessed by CD and NMR. Both analyses clearly indicate refolding of TC5b after processing. The CD spectra of the process input and output are depicted in Figure 7B. The spectra exhibit excellent agreement. A slight magnitude offset reflects putative concentration measurement error used in the mathematical transformation to mean residue molar ellipticity (MRME) units rather than inherent secondary structure differences. This conclusion is bolstered by inspection of the <sup>1</sup>H, <sup>15</sup>N HMQC 2D NMR data showing essentially perfect overlap between each identified residue (Figure 7C). Residues were identified from literature reports under the same buffer conditions. 26 Further, these data demonstrate recovery of high chemical shift dispersion, indicative of a folded structure, that had been lost upon DMSO exposure (Figure S2).

**Discussion.** The iFNP process was designed to enable higher therapeutic loadings using scalable production steps. Despite these potential benefits, the solvent requirements of iFNP are potentially detrimental to proteins with complex structures. The solubility of the stabilizing PAsp-b-PLA block copolymer requires the use of DMSO, which is known to denature many proteins. 15,27 Several studies have evaluated the effect of DMSO on the molecular interactions between a protein and its chemical environment. While at low concentrations of DMSO, the majority of proteins are found to be conformationally unaffected, they undergo a number of structural changes as DMSO concentration increases. Bagchi and colleagues studied the unfolding of proteins with  $\alpha$ -helical and  $\beta$ -sheet domains in the presence of aqueous DMSO.<sup>28–30</sup> Sedov et al. studied the unfolding of hen egg white lysozyme in mixtures of water with DMSO at different compositions.<sup>31</sup> These works motivate us to examine the capability of DMSO as a helix breaker and to apply these findings to better

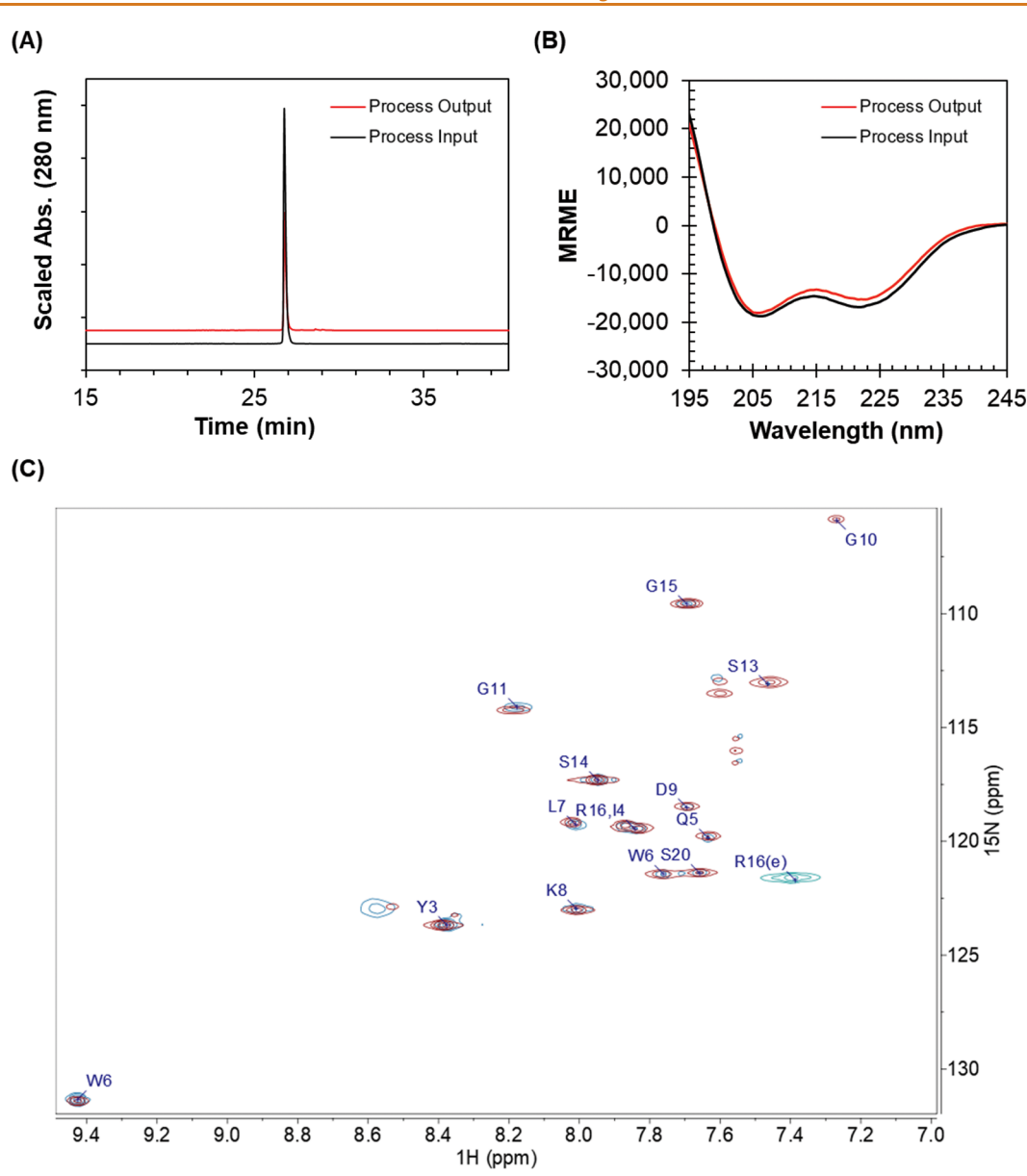


Figure 7. (A) HPLC chromatograms of purified  $^{15}$ N-TC5b (black line) and after iFNP processing (red line). (B) CD spectra before processing (black) and after processing to coated nanocarriers (red). Units are mean residue molar ellipticity. The slight offset is due to concentration measurement error rather than true confirmation changes, as supported by the 2D NMR characterization. (C) 2D SOFAST-HMQC spectra of purified  $^{15}$ N-TC5b before (dark blue contours) and after iFNP processing (red contours), showing good agreement between the two samples for all identified residues. The green contours for R16(e) correspond to the folded-in Arg side chain H $\varepsilon$ -N $\varepsilon$  peak, present for both samples.

understand protein behavior during iFNP processing. We developed a combined experimental and simulation approach to identify stability challenges when formulating new proteins. Evaluation of mid-process structural changes provided additional insight not possible by characterizing the final protein state alone.

NMR analysis demonstrated TC5b unfolding at 11 M (78 vol %) DMSO. This is in agreement with a study using vibrational CD analysis that found unfolding above 75 vol % DMSO using a more limited set of conditions. <sup>27</sup> Furthermore, our fully atomistic replica exchange molecular dynamics (REMD) simulations unequivocally confirmed the transition at this concentration, providing molecular level insight into structural changes. The large shifts of the order parameters  $C\alpha$  rmsd and W6S14 distance showed that TC5b unfolds at high

DMSO concentrations. The unfolded state also had a large radius of gyration and solvent-accessible surface area, indicating solvent penetration into TC5b that disturbed structural elements of the protein. The use of simulations identified the formation of a stabilizing salt bridge between the oppositely charged aspartic acid (D9) and arginine (R16) residues that would not have been detected by NMR analysis alone.

Molecular simulations indicated structural aspects that contributed to refolding behavior. In particular, the simulations showed that DMSO-induced unfolding does not lead to complete structural unraveling. In addition to the salt bridge, elements of TC5b's secondary structure such as the N-terminal  $\alpha$ -helix are also partially preserved. Computational studies have shown that this salt bridge formation can expedite the folding

kinetics of TC5b. To Consequently, the refolding of TC5b in the NC core or upon release may be enhanced due to the existence of the salt bridge in DMSO-induced unfolded structures. These findings suggest that biologics with stabilizing features such as salt bridges could have a higher likelihood of successful formulation by iFNP. Further, the survival of  $\alpha$ -helical character indicates that this structural feature may be an important predictor of successful refolding for other proteins used in iFNP. Examples of therapeutic proteins matching these structural features include cytokines such as interferon  $\alpha$  or interleukin-2 that consist of  $\alpha$ -helical bundles stabilized with disulfide bonds. This class of proteins could be employed for delivery by nanocarriers produced by iFNP for virology and oncology applications.  $^{32,33}$ 

The combination simulation-experiment approach to understanding protein folding and unfolding in encapsulation processes provides detailed insight guiding formulation development. However, the methods employed in this work do not capture all forms of instability, including protein aggregation due to unfolding. Clinical translation will require additional efforts to understand aggregation as well as chemical stability. The TC5b model employed in this work is a small protein with fast folding dynamics. Future work will be necessary to probe the impacts of slower folding dynamics and structural motifs such as  $\beta$ -sheets. Larger therapeutic proteins of interest would increase the demands on simulation resources, but there are a number of classes below 20 kDa that are tractable. This combined simulation-experiment approach has utility beyond its application to iFNP. For example, the double emulsion method for protein encapsulation has well-established liabilities for protein unfolding due to the use of organic solvents. 34-36 The application of simulations to understand the behavior of a protein therapeutic in this solvent system could guide selection of stabilizing additives from those proposed based on studies of model proteins if problems are identified in experimental work.<sup>3</sup>

While this work has developed protein characterization methods using an iFNP process that requires dissolution in DMSO, modifications to iFNP are being pursued to accommodate larger proteins that are irreversibly denatured by DMSO. A simple strategy to achieve this uses a four stream multi-inlet vortex mixer to segregate the biologic into an aqueous stream, limiting contact time with organic solvent. In this system, transient contact between dissolved protein and solvent occurs over the mixing and assembly time scales of 1.5 and 10–50 ms, respectively. Consideration of the kinetics of unfolding and refolding for larger proteins will be helpful. In addition, new experimental techniques to minimize solvent exposure through protein clustering hold promise to enable iFNP processing of more sensitive proteins.

# **CONCLUSIONS**

The formulation of proteins into nanocarriers can be used to enhance their therapeutic use. We have developed inverse Flash NanoPrecipitation as a scalable route to such formulations. While the process overcomes limitations in loading and encapsulation efficiency that have hindered the translation of existing approaches, the methods employed may alter the structural state of the protein therapeutic. Biologic stability is often difficult to monitor mid-process. We employed a combination of simulations and experimental techniques using a Trp-cage miniprotein, TCSb, as a model to assess unfolding and refolding across different processing steps. The

use of simulations and experimental techniques provided insights that each alone could not address. Unfolding in the iFNP input stream occurred, but TC5b refolded properly after processing. These results suggest that proteins with simple refolding mechanisms, particularly containing stabilizing features such as salt bridges, may be used in the iFNP process directly. We continue to develop modifications to iFNP that will expand the classes of proteins that can be released in an active manner. The methods employed here provide a path forward for evaluating the behavior of more complex proteins in encapsulation technologies through the application of simulations and experimental characterization.

## **METHODS**

**Experimental Methods.** *Materials.* DNA encoding the *de novo* expression enhancer protein (DEEP)—Trp-cage fusion protein (see seq 1) was ordered as a single gBlock from IDT.

Seq 1: MYGKLNDLLEDLQEVLKNLHKNWHGGKDNLHDVDNHLQNVIEDIHDFMQGGGSGGKLQEMMKEFQQVLDELNNHLQGGKHTVHHIEQNIKEIFHHLEELVHRGGGGGGSRMNLYIQWLKDGGPSSGRPPPS

Cloning primers as well as other chemicals used in the expression process were all purchased from Sigma-Aldrich (MilliporeSigma; St. Louis, MO). Reagent grade sodium phosphate monobasic and calcium nitrate tetrahydrate were also obtained from Sigma-Aldrich and were used as received. DMSO-d<sub>6</sub> and deuterium oxide were obtained from Cambridge Isotope Laboratories, Inc. (Andover, MA). Reagent grade sodium phosphate dibasic, reagent grade ammonium hydroxide (28–30% solution in water), HPLC grade tetrahydrofuran, HPLC grade methanol, ACS grade chloroform, and HPLC grade dimethylsulfoxide were obtained from Thermo Fisher Scientific (Waltham, MA). The trifluoroacetic acid (TFA) salt of the Trpcage variant TC5b (Asn-Leu-Tyr-Ile-Gln-Trp-Leu-Lys-Asp-Gly-Gly-Pro-Ser-Ser-Gly-Arg-Pro-Pro-Pro-Ser) with a purity of 95.4% was obtained from Genscript, Inc. (Piscataway, NJ). Molecular weight matched the theoretical value (2169.4) as determined by mass spectrometry. Poly(lactic acid)-b-poly(ethylene glycol) (100 DL, 5k mPEG) was a gift from Evonik GmbH (Essen, Germany). PAsp-b-PLA-b-PAsp was synthesized as described by Markwalter et al.9

Plasmid Construction, Protein Expression, Purification, and Chemical Cleavage of <sup>15</sup>N-TC5b. Using standard genetic engineering techniques, DNA coding DEEP-Trp-cage was cloned into a pET30 vector carrying kanamycin resistance. The plasmid was transformed into Escherichia coli, DH5a, minipreped, and sequenced with Sanger Sequencing (Genewiz). The sequenced plasmid was transformed into BL21(DE3) E. coli cells and plated on LB agar plates supplemented with 30 mg/L kanamycin. A single colony was picked and inoculated into 5 mL of LB (supplemented with kanamycin) and incubated overnight in a shaking incubator at 37 °C and 200 rpm. The following day, 1 L of LB containing 30 mg/L kanamycin was inoculated with 4 mL of the overnight grown culture and allowed to grow to  $OD_{600}$  = 0.5. Cells were centrifuged, washed with a solution of minimal M9 salts, and resuspended in 1 L of minimal M9 media supplemented with 1 g of <sup>15</sup>NH<sub>4</sub>Cl. Overexpression was initiated by the addition of IPTG to a final concentration of 0.5 mM. The temperature was decreased to 18 °C, and cells were grown for an additional ~15 h. Cells were pelleted by centrifugation at 5000 rcf for 30 min and stored at -80 °C until further use. Lysis was initiated by resuspension of the cell pellet in buffer A (50 mM Tris, 300 mM NaCl at pH 8) and a five cycle passage through Emulsiflex C3 homogenizer operating at 15,000 psi. Lysed cells were centrifuged at 35,000 rcf for 1 h, and the supernatant was filtered with a 0.45  $\mu m$  PVDF syringe filter.

The clarified lysate was applied onto a pre-equilibrated Ni column and purified using the following buffers: buffer A as equilibration/wash buffer and elution buffer (50 mM Tris, 300 mM NaCl, 500 mM imidazole at pH 8). The eluted peak was supplemented with 6 M guanidine—HCl, and CNBr cleavage was initiated following a

previously reported method.<sup>40</sup> The cleavage reaction was dried using a SpeedVac system connected to a cold trap (Savant, SC110).

Dried samples were reconstituted in water and further purified on an Agilent 1100 HPLC equipped with Zorbax 300SB-C18, 5  $\mu$ m, 9.4  $\times$  250 mm column using the following protocol: 20 min at 20% B followed by 20 min gradient 20–34% B at a flow rate of 3 mL/min (A, water; B, MeCN; both supplemented with 0.1% trifluoroacetic acid). The TCSb peak was collected, lyophilized, and confirmed by mass spectrometry, liquid chromatography, and circular dichroism.

DMSO Titration Experiment by NMR. Solutions of <sup>15</sup>N-TC5b were prepared in deionized water and DMSO at 1 mM. These solutions were mixed to achieve the target compositions summarized in Table 1. A seventh solution was prepared in 25 mM phosphate buffer, pH

Table 1. DMSO Titration Conditions Used to Evaluate Unfolding of TC5b in the iFNP Input Stream<sup>a</sup>

condition	DMSO (M)	DMSO (vol %)
6	14.08	100
5	13.5	94
4	11	78
3	5	36
2	1	7
1	0	0

<sup>a</sup>The remainder of the solution content was comprised of deionized water.

6.8, as a baseline for comparison to TC5b released from the NCs after processing. The small volume ( $\sim$ 100  $\mu$ L) samples were prepared in 1.7 mm o.d. capillaries, which were inserted into 5/3 mm o.d. container tubes (New Era Enterprises, Inc., Vineland, NJ). A small amount of D2O between the walls provided the lock signal. All experiments were run at 800 MHz on a Bruker Avance III HD instrument equipped with a custom-made 5 mm QCI-F cryoprobe  $(^{1}H)^{19}F/^{13}C/^{15}N/^{2}H)$  at controlled temperature, typically at 295 K. Other temperatures (277, 313, and 333 K) were also tested. 1D proton experiments were done using excitation sculpting water suppression (ES); 2D SOFAST-HMQC (SF) experiments were used to collect <sup>15</sup>N, <sup>1</sup>H correlations. <sup>41,42</sup> Additional TOCSY (80 ms spinlock time) and NOESY (300 ms and 700 ms mixing time) experiments were run on samples with 0% DMSO and 94% DMSO added, respectively. All data processing and data analysis were done off-line in MNova (v.12, MestreLab Research S.L., Santiago de Compostela, Spain).

*TC5b Formulation by iFNP*. Inverse NCs were prepared as previously described. <sup>9,43</sup> In brief, solutions of PAsp<sub>Sk</sub>-b-PLA<sub>10k</sub>-b-PAsp<sub>5k</sub> block copolymer and TC5b were prepared in DMSO at 12.5 mg/mL. The solvent and antisolvent streams for mixing were prepared from these stock solutions as follows. The solvent stream contained 6 mg/mL of the block copolymer and 4 mg/mL of TC5b. Early screening produced stable particles at 50% loading, but this was lowered to 40% to reduce material usage. The solvent composition was 95% DMSO and 5% deionized water with a total volume of 500  $\mu$ L. The antisolvent stream contained 500  $\mu$ L of chloroform (CHCl<sub>3</sub>) and 50  $\mu$ L of a 30.8 mg/mL solution of Ca(NO<sub>3</sub>)<sub>2</sub> in methanol, which corresponds to a 1:1 charge ratio with the acid groups on PAsp. A collection bath containing 4 mL of CHCl<sub>3</sub> and a stirbar was prepared in a 20 mL scintillation vial. The two streams were rapidly mixed in a CIJ mixer, and the NC dispersion was characterized by dynamic light scattering (DLS) as described below. 43 A 2.67 mg/mL solution of ammonia in methanol was prepared gravimetrically using ammonium hydroxide. Fifty microliters of the ammonia solution was added dropwise to the rapidly stirring NC dispersion. This corresponds to 0.6 equiv with respect to the PAsp acid residues. The dispersion was aged for 30 min to allow crosslinking of the PAsp.4-

Particle size was characterized by DLS using a Zetasizer Nano ZS (Malvern, Worcestershire, UK) at 25 °C by diluting each sample 10-fold with CHCl<sub>3</sub>. Size distributions were determined from a CONTIN

analysis implemented by the Zetasizer software. The polydispersity index was obtained from the autocorrelation function as implemented by the Zetasizer software. Values of 0.1 are generally obtained for monodisperse particles. 45,46

The NC dispersion was extracted with 3.5 mL of 150 mM brine to remove DMSO and unencapsulated TC5b. The organic layer was separated from the aqueous stream and sampled for DLS characterization. The aqueous stream was assayed to quantify the encapsulation efficiency of the iFNP step. <sup>47</sup> A solution of PLA-b-PEG at 10 mg/mL in THF was added (0.188 mL) to the NC dispersion such that the mass ratio of this PEG stabilizer to inverse NC was 0.5:1. The NP dispersion was diluted 50% with THF, and a solvent exchange process was carried out by rotary evaporation whereby the solution was concentrated to 1 mL and then diluted with 8 mL of THF. This put-and-take distillation was repeated three times, and the NC dispersion was then concentrated to 0.75 mL as a THF solution. The particle stability to this processing was again assessed by DLS.

The coating process employed rapid mixing in a CIJ against an equal volume of deionized water. The quench bath contained 5 mL of deionized water. The coated NCs were characterized by DLS and zeta-potential measurements. The zeta potential was determined using a disposable folded capillary (Malvern Panalytical, DTS1070) in 0.1× phosphate-buffered saline. Transmission electron micrographs were generated using a TALOS F200x scanning/transmission electron microscope. NC suspensions after coating were washed on 100 kDa Amicon ultrafilters (Amicon, Millipore-Sigma; St. Louis, MO) to remove unencapsulated material and were freeze dried onto a copper TEM grid (300 mesh carbon film, Electron Microscopy Sciences). Vapor-phase ruthenium staining was carried out by generating ruthenium tetroxide from ruthenium dioxide using sodium metaperiodate. 48 The headspace in an enclosed chamber was allowed to equilibrate for 5 min, and then the grids were added for 1-2 min staining exposure.

Characterization of iFNP-Processed TC5b. TC5b was formulated as described above, with slight modifications. Residual poly(aspartic acid) homopolymer was first removed from the PAsp-b-PLA block copolymer by a water precipitation process. PAsp-b-PLA-b-PAsp was dissolved in DMSO and added dropwise into water. The suspension was rinsed extensively on a 100 kDa ultrafilter and then lyophilized. The purified block copolymer was used as above, but ammonia was reduced to 0.5 equiv. Additionally, the brine extraction was repeated a second time to ensure complete DMSO removal. Coating proceeded as described above.

Free TC5b, which had been encapsulated by iFNP but diffused from the NCs during coating, was separated from the coated NCs using 100 kDa molecular weight cut-off ultrafilters that had been rinsed with water to remove membrane preservatives. For CD studies, the residual THF was removed by rotary evaporation (37 °C for 2 h) followed by addition of phosphate buffer (pH 6.8) to a final concentration of 25 mM. The circular dichroism spectra were collected as described below. For NMR studies of released TC5b, residual THF was removed by ultrafiltration on a 3 kDa ultrafilter. The retained TC5b was washed with 25 mM phosphate buffer (pH 6.8) and recovered with filter rinses to a final concentration of about 1.5 mg/mL. NMR spectra were collected as described above and compared with the input (unprocessed) TC5b in phosphate buffer. The HPLC purity of the released TC5b was assayed as described above.

Circular Dichroism for Structural Characterization of Trp-Cage. CD spectra from 190 to 250 nm were collected at 0.5 nm increments using a Chirascan spectrometer (Applied Photophysics, Leatherhead, UK). Temperature was maintained at 22 °C using a TC 125 temperature controller (Quantum Northwest, Liberty Lake, WA) and a Julabo AWC100 recirculating cooler. Spectra were baseline subtracted and then smoothed using Chirascan software. Molar ellipticity values were determined from the raw CD data and the measured TC5b molarity from absorbance at 280 nm.

**Computational Methods.** *Protein Initial Configurations and Equilibration.* The NMR structure of Trp-cage miniprotein variant TC5b was taken from the Research Collaboratory for Structural

Bioinformatics Protein Data Bank (PDB ID code 1L2Y). <sup>16</sup> TC5b was modeled using a modified version of the Amber03 force field (Amber03w), compatible with the TIP4P/2005 model of water. <sup>20–22</sup> DMSO was modeled using the generalized Amber force field (GAFF). <sup>23</sup> Electroneutrality of the system was achieved by adding a chloride ion to the system to counter the +1 net charge on the protein.

The starting configurations for TC5b were sampled from a 3  $\mu$ s Trp-cage simulation at 298 K and 1 bar in pure water. These configurations were then solvated in 0, 1, 5, 11, and 13.5 M DMSO/ water mixtures and pure DMSO. The systems were briefly energy minimized using the steepest descent method in order to ensure there were no atomic overlaps. The solvent was then equilibrated by a 3 ns NVT MD simulation using the Berendsen thermostat while position-restraining the protein.<sup>49</sup> After the solvent was equilibrated, the position restraints were removed and the system was equilibrated using the Berendsen thermostat and barostat for 1 ns in the isothermal-isobaric ensemble. Water molecules were constrained using the SETTLE algorithm, and the linear constraint solver (LINCS) was applied to the bonds in the protein. 50,51 The shortrange interactions were truncated at 1 nm, and standard long-range dispersion corrections were applied to energy and pressure. The particle mesh Ewald (PME) technique with a 0.1 nm grid spacing was used to treat the long-range electrostatic interactions.

Replica Exchange Molecular Dynamics Simulations. The REMD simulations were performed using the GROMACS simulation package at 42 temperatures ranging from 286.5 to 483.5 K (1 and 5 M) and 286.5 to 519.5 K (11 and 13.5 M and pure DMSO). The trajectories for 0 M were obtained from our previous work. S3,54 Replica temperatures were determined by running several iterations of 100 ps long REMD simulations. The distribution of replica temperatures was chosen to achieve a 20–25% acceptance rate for exchanges between adjacent states that were attempted every 2 ps.

The REMD simulations were carried out in the isothermal-isobaric ensemble using the leapfrog algorithm with a 2 fs time step. The temperature and pressure were maintained using the Nose–Hoover thermostat (0.2 ps time constant) and the Parrinello–Rahman barostat (2 ps time constant), respectively. 55–57

Simulations were run for 2.5  $\mu$ s per replica for the 1, 5, and 11 M systems and 1.9  $\mu$ s for the 13.5 M and pure DMSO systems. After their convergence was ensured, the last 1.5  $\mu$ s of the trajectories was used for the analysis of the 1, 5, and 11 M systems, and the last 1  $\mu$ s was used for the 13.5 M and pure DMSO systems. In these simulations, the lengths of the production runs correspond to at least 15 times the correlation time of the fraction of folded proteins in all replicas, where the correlation time is defined as the value at which the time correlation function of the fraction of folded proteins in all replicas crosses zero for the first time. In concentrated ionic solutions (1, 5, and 11 M), longer production times were used as slower dynamics frustrate sampling in these systems.

Thermodynamic and Structural Analysis. In order to monitor the DMSO-induced perturbations in TC5b structure, we constructed the free energy surfaces associated with the order parameters  $\alpha$ -carbon root-mean-squared deviation from the folded NMR reference structure (C $\alpha$  rmsd) and the distance between the tryptophan (W6) and serine (S14) residues of TC5b (W6S14 distance). The order parameters were chosen based on our previous work. 53,54 Analysis of the C $\alpha$  rmsd and W6–S14 distance distributions of TC5b in pure water at 300 K and the corresponding free energy surface based on these order parameters provides a natural definition of the ensemble of folded configurations as structures with C $\alpha$  rmsd < 0.3 nm and W6S14 distance < 0.42 nm.  $^{53}$ 

The electrostatic interactions between oppositely charged residues aspartic acid (D9) and arginine (R16) stabilize the folded structure of TC5b. We investigated the formation of a salt bridge between these residues by monitoring the shortest distance between the charged oxygen and nitrogen atoms of D9 and R16, respectively. The salt bridge was considered to be formed when the distance between the two residues was less than 0.5 nm. We also computed the solvent-

accessible surface area and the radius of gyration  $(R_g)$  using the utilities distributed with GROMACS.

### **ASSOCIATED CONTENT**

# **5** Supporting Information

The Supporting Information is available free of charge at https://pubs.acs.org/doi/10.1021/acsnano.0c06056.

Additional characterization of the TC5b by CD; supplemental HSQC-NMR results; supplemental free energy surface simulations results; probability distribution of salt bridge distance (PDF)

# **AUTHOR INFORMATION**

# **Corresponding Authors**

Robert K. Prud'homme — Department of Chemical and Biological Engineering, Princeton University, Princeton, New Jersey 08544, United States; orcid.org/0000-0003-2858-0097; Email: prudhomm@princeton.edu

Pablo G. Debenedetti — Department of Chemical and Biological Engineering, Princeton University, Princeton, New Jersey 08544, United States; orcid.org/0000-0003-1881-1728; Email: pdebene@princeton.edu

### **Authors**

Chester E. Markwalter — Department of Chemical and Biological Engineering, Princeton University, Princeton, New Jersey 08544, United States; orcid.org/0000-0002-0247-5881

Betul Uralcan — Department of Chemical and Biological Engineering, Princeton University, Princeton, New Jersey 08544, United States; orcid.org/0000-0002-0669-8441

István Pelczer – Department of Chemistry, Princeton University, Princeton, New Jersey 08544, United States; orcid.org/0000-0002-7806-6101

Shlomo Zarzhitsky — Department of Chemistry, Princeton University, Princeton, New Jersey 08544, United States Michael H. Hecht — Department of Chemistry, Princeton University, Princeton, New Jersey 08544, United States

Complete contact information is available at: https://pubs.acs.org/10.1021/acsnano.0c06056

# **Author Contributions**

C.E.M. and B.U. contributed equally to this work. B.U. carried out the simulations. S.Z. produced the Trp cage construct. C.M. purified, formulated, and prepared samples of the construct. I.P. designed, conducted, and completed the analysis of the NMR experiments. All authors contributed to the design and planning of the experiments. The manuscript was written through contributions of all authors. All authors have given approval to the final version of the manuscript.

#### Notes

1

The authors declare the following competing financial interest(s): R.K.P. has a financial interest in Optimeos Life Sciences.

### **ACKNOWLEDGMENTS**

The authors acknowledge the use of the Biophysics and NMR core facilities in the Princeton Department of Chemistry. The authors acknowledge the use of Princeton's Imaging and Analysis Center, which is partially supported by the Princeton Center for Complex Materials, a National Science Foundation (NSF)-MRSEC program (DMR-1420541). The authors wish

to thank B. Wilson for his assistance in staining particles for TEM imaging, and R. Pagels for many helpful discussions. R. Pagels generously supplied the PAsp-b-PLA-b-PAsp block copolymer used in this work. This work used the Extreme Science and Engineering Discovery Environment (XSEDE), which is supported by National Science Foundation Grant No. ACI-1548562, and Princeton Research Computing, a consortium of groups including the Princeton Institute for Computational Science and Engineering (PICSciE) and the Office of Information Technology's High Performance Computing Center and Visualization Laboratory at Princeton University. Funding for C.E.M. was provided by Optimeos Life Sciences, in which R.K.P. has a financial interest. C.E.M. was partially funded by a PhRMA Foundation Pre-Doctoral Fellowship in Pharmaceutics. S.Z. was funded by NSF Grant Nos. MCB-1409402 and MCB-1947720.

# **REFERENCES**

- (1) Walsh, G. Biopharmaceutical Benchmarks 2018. *Nat. Biotechnol.* **2018**, *36*, 1136–1147.
- (2) Anselmo, A. C.; Gokarn, Y.; Mitragotri, S. Non-Invasive Delivery Strategies for Biologics. *Nat. Rev. Drug Discovery* **2019**, *18*, 19–40.
- (3) Yu, M.; Wu, J.; Shi, J.; Farokhzad, O. C. Nanotechnology for Protein Delivery: Overview and Perspectives. *J. Controlled Release* **2016**, 240, 24–37.
- (4) Fosgerau, K.; Hoffmann, T. Peptide Therapeutics: Current Status and Future Directions. *Drug Discovery Today* **2015**, 20, 122–128.
- (5) Mitragotri, S.; Burke, P. A.; Langer, R. Overcoming the Challenges in Administering Biopharmaceuticals: Formulation and Delivery Strategies. *Nat. Rev. Drug Discovery* **2014**, *13*, 655–672.
- (6) Yu, M.; Benjamin, M. M.; Srinivasan, S.; Morin, E. E.; Shishatskaya, E. I.; Schwendeman, S. P.; Schwendeman, A. Battle of Glp-1 Delivery Technologies. *Adv. Drug Delivery Rev.* **2018**, *130*, 113–130.
- (7) Du, A. W.; Stenzel, M. H. Drug Carriers for the Delivery of Therapeutic Peptides. *Biomacromolecules* **2014**, *15*, 1097–1114.
- (8) Pagels, R. F.; Prud'homme, R. K. Polymeric Nanoparticles and Microparticles for the Delivery of Peptides, Biologics, and Soluble Therapeutics. *J. Controlled Release* **2015**, 219, 519–535.
- (9) Markwalter, C. E.; Pagels, R. F.; Hejazi, A. N.; Gordon, A. G. R.; Thompson, A. L.; Prud'homme, R. K. Polymeric Nanocarrier Formulations of Biologics Using Inverse Flash Nanoprecipitation. *AAPS J.* **2020**, *22*, 18.
- (10) D'Addio, S. M.; Prud'homme, R. K. Controlling Drug Nanoparticle Formation by Rapid Precipitation. *Adv. Drug Delivery Rev.* **2011**, *63*, 417–426.
- (11) Johnson, B. K.; Prud'homme, R. K. Mechanism for Rapid Self-Assembly of Block Copolymer Nanoparticles. *Phys. Rev. Lett.* **2003**, *91*, 118302.
- (12) Pagels, R. F.; Edelstein, J.; Tang, C.; Prud'homme, R. K. Controlling and Predicting Nanoparticle Formation by Block Copolymer Directed Rapid Precipitations. *Nano Lett.* **2018**, *18*, 1139–1144.
- (13) Saad, W. S.; Prud'homme, R. K. Principles of Nanoparticle Formation by Flash Nanoprecipitation. *Nano Today* **2016**, *11*, 212–227.
- (14) Putney, S.; Burke, P. Improving Protein Therapeutics with Sustained-Release Formulations. *Nat. Biotechnol.* **1998**, *16*, 153–157.
- (15) Kazandjian, R.; Dordick, J. S.; Klibanov, A. M. Enzymatic Analyses in Organic Solvents. *Biotechnol. Bioeng.* **1986**, 28, 417–421.
- (16) Neidigh, J. W.; Fesinmeyer, R. M.; Andersen, N. H. Designing a 20-Residue Protein. *Nat. Struct. Biol.* **2002**, *9*, 425–430.
- (17) Neuweiler, H.; Doose, S.; Sauer, M. A Microscopic View of Miniprotein Folding: Enhanced Folding Efficiency through Formation of an Intermediate. *Proc. Natl. Acad. Sci. U. S. A.* **2005**, *102*, 16650.

- (18) Paschek, D.; Hempel, S.; Garcia, A. E. Computing the Stability Diagram of the Trp-Cage Miniprotein. *Proc. Natl. Acad. Sci. U. S. A.* **2008**, *105*, 17754–17759.
- (19) Qiu, L.; Pabit, S. A.; Roitberg, A. E.; Hagen, S. J. Smaller and Faster: The 20-Residue Trp-Cage Protein Folds in 4 Microseconds. *J. Am. Chem. Soc.* **2002**, *124*, 12952–12953.
- (20) Abascal, J. L. F.; Vega, C. A General Purpose Model for the Condensed Phases of Water: Tip4p/2005. *J. Chem. Phys.* **2005**, *123*, 234505.
- (21) Best, R. B.; Mittal, J. Protein Simulations with an Optimized Water Model: Cooperative Helix Formation and Temperature-Induced Unfolded State Collapse. *J. Phys. Chem. B* **2010**, *114*, 14916–14923.
- (22) Duan, Y.; Wu, C.; Chowdhury, S.; Lee, M. C.; Xiong, G.; Zhang, W.; Yang, R.; Cieplak, P.; Luo, R.; Lee, T.; Caldwell, J.; Wang, J.; Kollman, P. A Point-Charge Force Field for Molecular Mechanics Simulations of Proteins Based on Condensed-Phase Quantum Mechanical Calculations. *J. Comput. Chem.* **2003**, *24*, 1999–2012.
- (23) Wang, J.; Wolf, R. M.; Caldwell, J. W.; Kollman, P. A.; Case, D. A. Development and Testing of a General Amber Force Field. *J. Comput. Chem.* **2004**, *25*, 1157–1174.
- (24) Zarzhitsky, S.; Jiang, A.; Stanley, E.; Hecht, M. Harnessing Synthetic Biology to Enhance Heterologous Protein Expression. *Protein Sci.* **2020**, *29*, 1698–1706.
- (25) Struthers, M.; Ottesen, J. J.; Imperiali, B. Design and Nmr Analyses of Compact, Independently Folded Bba Motifs. *Folding Des.* **1998**, 3, 95–103.
- (26) Rogne, P.; Ozdowy, P.; Richter, C.; Saxena, K.; Schwalbe, H.; Kuhn, L. T. Atomic-Level Structure Characterization of an Ultrafast Folding Mini-Protein Denatured State. *PLoS One* **2012**, *7*, e41301.
- (27) Copps, J.; Murphy, R. F.; Lovas, S. Vcd Spectroscopic and Molecular Dynamics Analysis of the Trp-Cage Miniprotein Tc5b. *Biopolymers* **2007**, *88*, 427–437.
- (28) Roy, S.; Jana, B.; Bagchi, B. Dimethyl Sulfoxide Induced Structural Transformations and Non-Monotonic Concentration Dependence of Conformational Fluctuation around Active Site of Lysozyme. *J. Chem. Phys.* **2012**, *136*, 115103–115103.
- (29) Roy, S.; Bagchi, B. Chemical Unfolding of Chicken Villin Headpiece in Aqueous Dimethyl Sulfoxide Solution: Cosolvent Concentration Dependence, Pathway, and Microscopic Mechanism. *J. Phys. Chem. B* **2013**, *117*, 4488–4502.
- (30) Roy, S.; Bagchi, B. Comparative Study of Protein Unfolding in Aqueous Urea and Dimethyl Sulfoxide Solutions: Surface Polarity, Solvent Specificity, and Sequence of Secondary Structure Melting. *J. Phys. Chem. B* **2014**, *118*, 5691–5697.
- (31) Sedov, I. A.; Magsumov, T. I. Molecular Dynamics Study of Unfolding of Lysozyme in Water and Its Mixtures with Dimethyl Sulfoxide. *J. Mol. Graphics Modell.* **2017**, *76*, 466–474.
- (32) Anderson, P. M.; Hanson, D. C.; Hasz, D. E.; Halet, M. R.; Blazar, B. R.; Ochoa, A. C. Cytokines in Liposomes: Preliminary Studies with Il-1, Il-2, Il-6, Gm-Csf and Interferon-Γ. *Cytokine+* **1994**, *6*, 92–101.
- (33) Lipiäinen, T.; Peltoniemi, M.; Sarkhel, S.; Yrjönen, T.; Vuorela, H.; Urtti, A.; Juppo, A. Formulation and Stability of Cytokine Therapeutics. *J. Pharm. Sci.* **2015**, *104*, 307–326.
- (34) Schwendeman, S. P.; Shah, R. B.; Bailey, B. A.; Schwendeman, A. S. Injectable Controlled Release Depots for Large Molecules. *J. Controlled Release* **2014**, *190*, 240–253.
- (35) Teekamp, N.; Duque, L. F.; Frijlink, H. W.; Hinrichs, W. L. J.; Olinga, P. Production Methods and Stabilization Strategies for Polymer-Based Nanoparticles and Microparticles for Parenteral Delivery of Peptides and Proteins. *Expert Opin. Drug Delivery* **2015**, 12, 1311–1331.
- (36) Ye, M.; Kim, S.; Park, K. Issues in Long-Term Protein Delivery Using Biodegradable Microparticles. *J. Controlled Release* **2010**, *146*, 241–260.
- (37) Morlock, M.; Koll, H.; Winter, G.; Kissel, T. Microencapsulation of Rh-Erythropoietin, Using Biodegradable Poly (D,L-

- Lactide-Co-Glycolide): Protein Stability and the Effects of Stabilizing Excipients. Eur. J. Pharm. Biopharm. 1997, 43, 29–36.
- (38) Markwalter, C. E.; Prud'homme, R. K. Design of a Small-Scale Multi-Inlet Vortex Mixer for Scalable Nanoparticle Production and Application to the Encapsulation of Biologics by Inverse Flash Nanoprecipitation. *J. Pharm. Sci.* **2018**, *107*, 2465–2471.
- (39) Johnston, K. P.; Maynard, J. A.; Truskett, T. M.; Borwankar, A. U.; Miller, M. A.; Wilson, B. K.; Dinin, A. K.; Khan, T. a.; Kaczorowski, K. J. Concentrated Dispersions of Equilibrium Protein Nanoclusters That Reversibly Dissociate into Active Monomers. *ACS Nano* 2012, *6*, 1357–1369.
- (40) Andreev, Y. A.; Kozlov, S. A.; Vassilevski, A. A.; Grishin, E. V. Cyanogen Bromide Cleavage of Proteins in Salt and Buffer Solutions. *Anal. Biochem.* **2010**, *407*, 144–146.
- (41) Hwang, T. L.; Shaka, A. J. Water Suppression That Works. Excitation Sculpting Using Arbitrary Wave-Forms and Pulsed-Field Gradients. *J. Magn. Reson., Ser. A* 1995, 112, 275–279.
- (42) Schanda, P.; Brutscher, B. Very Fast Two-Dimensional Nmr Spectroscopy for Real-Time Investigation of Dynamic Events in Proteins on the Time Scale of Seconds. *J. Am. Chem. Soc.* **2005**, 127, 8014—8015.
- (43) Markwalter, C. E.; Pagels, R. F.; Wilson, B. K.; Ristroph, K. D.; Prud'homme, R. K. Flash Nanoprecipitation for the Encapsulation of Hydrophobic and Hydrophilic Compounds in Polymeric Nanoparticles. *J. Vis. Exp.* **2019**, No. e58757.
- (44) Pagels, R. F.; Prud'homme, R. K. Inverse Flash Nano-precipitation for Biologics Encapsulation: Nanoparticle Formation and Ionic Stabilization in Organic Solvents. In Control of Amphiphile Self-Assembling at the Molecular Level: Supra-Molecular Assemblies with Tuned Physicochemical Properties for Delivery Applications; American Chemical Society: Washington, D.C., 2017; Vol. 1271, pp 249–274.

  (45) Frisken, B. J. Revisiting the Method of Cumulants Court and Control of Company of Properties Pater Applications (1997).
- (45) Frisken, B. J. Revisiting the Method of Cumulants for the Analysis of Dynamic Light-Scattering Data. *Appl. Opt.* **2001**, *40*, 4087–4091.
- (46) Sauer, B. B.; Stock, R. S.; Lim, K. H.; Ray, W. H. Polymer Latex Particle Size Measurement through High-Speed Dieletric Spectroscopy. *J. Appl. Polym. Sci.* **1990**, *39*, 2419–2441.
- (47) Markwalter, C. E.; Prud'homme, R. K. Inverse Flash Nanoprecipitation for Biologics Encapsulation: Understanding Process Losses via an Extraction Protocol. In Control of Amphiphile Self-Assembling at the Molecular Level: Supra-Molecular Assemblies with Tuned Physicochemical Properties for Delivery Applications; American Chemical Society: Washington, D.C., 2017; Vol. 1271, pp 275–296.
- (48) Trent, J. S.; Scheinbeim, J. I.; Couchman, P. R. Ruthenium Tetraoxide Staining of Polymers for Electron Microscopy. *Macromolecules* 1983, 16, 589–598.
- (49) Berendsen, H. J. C.; Postma, J. P. M.; van Gunsteren, W. F.; DiNola, A.; Haak, J. R. Molecular Dynamics with Coupling to an External Bath. *J. Chem. Phys.* **1984**, *81*, 3684–3690.
- (50) Hess, B. P-Lincs: A Parallel Linear Constraint Solver for Molecular Simulation. *J. Chem. Theory Comput.* **2008**, *4*, 116–122.
- (51) Miyamoto, S.; Kollman, P. A. Settle: An Analytical Version of the Shake and Rattle Algorithm for Rigid Water Models. *J. Comput. Chem.* **1992**, *13*, 952–962.
- (52) Essmann, U.; Perera, L.; Berkowitz, M. L.; Darden, T.; Lee, H.; Pedersen, L. G. A Smooth Particle Mesh Ewald Method. *J. Chem. Phys.* **1995**, *103*, 8577–8593.
- (53) Uralcan, B.; Debenedetti, P. G. Computational Investigation of the Effect of Pressure on Protein Stability. *J. Phys. Chem. Lett.* **2019**, *10*, 1894–1899.
- (54) Uralcan, B.; Kim, S. B.; Markwalter, C. E.; Prud'homme, R. K.; Debenedetti, P. G. A Computational Study of the Ionic Liquid-Induced Destabilization of the Miniprotein Trp-Cage. *J. Phys. Chem. B* **2018**, *122*, 5707–5715.
- (55) Hoover, W. G. Canonical Dynamics: Equilibrium Phase-Space Distributions. *Phys. Rev. A: At., Mol., Opt. Phys.* **1985**, 31, 1695–1697. (56) Nosé, S. A Unified Formulation of the Constant Temperature Molecular Dynamics Methods. *J. Chem. Phys.* **1984**, 81, 511–519.

(57) Parrinello, M.; Rahman, A. Polymorphic Transitions in Single Crystals: A New Molecular Dynamics Method. *J. Appl. Phys.* **1981**, *52*, 7182–7190.